Thermal and Solvent-Isotope Effects on the Flagellar Rotary Motor near Zero Load

Thermal and Solvent-Isotope Effects on the Flagellar Rotary Motor near Zero Load

Junhua Yuan and Howard C. Berg*
Department of Molecular and Cellular Biology, Harvard University, Cambridge, Massachusetts

ABSTRACT In *Escherichia coli*, the behavior of the flagellar rotary motor near zero load can be studied by scattering light from nanogold spheres attached to proximal hooks of cells lacking flagellar filaments. We used this method to monitor changes in speed when cells were subjected to changes in temperature or shifted from a medium made with H_2O to one made with D_2O. In H_2O, the speed increased with temperature in a near-exponential manner, with an activation enthalpy of 52 ± 4 kJ/mol (12.0 ± 1.0 kcal/mol). In D_2O, the speed increased in a similar manner, with an activation enthalpy of 50 ± 4 kJ/mol. The speed in H_2O was higher than that in D_2O by a factor of 1.53 ± 0.14. We performed comparison studies of variations in temperature and solvent isotope, using motors operating at high loads. The variations were small, consistent with previous observations. The implications of these results for proton translocation are discussed.

INTRODUCTION

Bacterial flagella are helical propellers driven by reversible rotary motors embedded in the cell wall. In *Escherichia coli*, the motor is powered by a transmembrane proton flux (1) that flows through two channels in torque-generating units composed of four copies of MotA and two copies of MotB, elements of the stator (2). High-resolution structures are not yet available for these channels, but their organization has been mapped by genetic and biochemical means (3–7). The residue Asp-32 of MotB near the cytoplasmic end of each channel has been shown to be essential (8). The protonation and subsequent deprotonation of Asp-32 are thought to drive conformational changes that exert forces on the periphery of the rotor via electrostatic interactions between MotA and the rotor protein FliG (9).

Measurements of the torque-speed relationship provided a crucial test of models for motor rotation (1,2). In *E. coli*, motor torque falls ~10% between 0 and ≈160 Hz (at room temperature) and then drops rapidly to 0 at ≈300 Hz (10,11). The properties of the motor in the regimes of high load (low speed) and low load (high speed) are distinctive. In the regime of high load, the motor operates near thermodynamic equilibrium, where rates of proton translocation or movement of mechanical components are not rate-limiting. The motor torque is independent of temperature, and solvent-isotope effects are small (12). In the regime of low load, the motor operates far from thermodynamic equilibrium, and rates of proton translocation or movement of mechanical components are limiting. It is of interest to study the motor in this regime, where kinetics matter. Proton flux and motor rotation are tightly coupled (13). Studies of thermal and isotope effects on motor rotation near zero load provide important information about the proton translocation process in the absence of complications due to effects of load.

Detailed studies of thermal effects on motor rotation have been carried out only in the high-load regime (12). Measurements of motor rotation under high to medium loads have been made at three temperatures (22.7°C, 17.7°C, and 15.8°C (11)). Measurements of motor rotation near zero load have been made at 11°C, 16°C, and 23°C by electrorotation of tethered cells (10). Measurements of solvent-isotope effects have been made under high to medium loads (12,14), with the lowest load studied resulting from 0.36-μm-diameter latex beads attached to filament stubs. No direct measurements of solvent-isotope effects have been made for motors near zero load. In recent studies, nanogold spheres were attached to the hooks of mutant *E. coli* cells lacking flagellar filaments, and the motion of individual spheres was followed by laser dark-field microscopy to enable a systematic investigation of the motor near zero load (15,16). Here, we apply this technique to measure speed variations of the motor near zero load within a temperature range of 9–37°C in both H_2O and D_2O.

MATERIALS AND METHODS

Media and bacteria

The motility medium in H_2O was 10 mM potassium phosphate, 0.1 mM EDTA, 10 mM lactate at pH 7.0. A buffer of identical ionic composition was made in D_2O (catalog no. 15188, 99.8%, Aldrich, St. Louis, MO) at pD 7.5. pD was measured with a pH meter by adding 0.44 units to the reading (17). Viscosities of the motility media made in H_2O and D_2O were obtained from previous studies (12,14), yielding a ratio of viscosity $D_2O/H_2O = 1.22$ at 23°C. For studies near zero load, we used *E. coli* strain JY25 (*ΔcheY, ΔfliC*), which lacks flagellar filaments and rotates its motors exclusively counterclockwise. It was derived from the wild-type strain RP437 (18) by previously described methods (15). For studies at high load, we used a JY25 strain that carries in addition the low-copy-number plasmid pKAF131, which expresses the *fliC* sticky allele. Cells were grown

Submitted December 1, 2009, and accepted for publication January 22, 2010.

*Correspondence: hberg@mcb.harvard.edu

Editor: Yale E. Goldman.

0006-3495/10/05/2121/6 $2.00

doi: 10.1016/j.bpj.2010.01.061

at 33°C in T-broth (1% tryptone, 0.5% NaCl) supplemented with 10% L-broth (1% tryptone, 0.5% NaCl, 0.5% yeast extract) and the appropriate antibiotics, to $OD_{600} \approx 0.5$. The cells were washed twice and resuspended to the same optical density in motility medium. They were used immediately for experiment or stored at 4°C for up to 1 h.

Sample preparation and microscopy

For studies near zero load, gold spheres (60 nm diameter, catalog no. 15709; Ted Pella, Inc., Redding, CA) were attached to hooks following a previously described procedure (15). For studies at high load, cells were sheared to truncate flagella by passing 1 mL of the washed-cell suspension 70 times between two syringes equipped with 26-gauge needles and connected by a 7-cm length of polyethylene tubing (0.58 mm i.d., catalog no. 427411; Becton Dickinson, Waltham, MA). Then, 1.0-μm-diameter polystyrene latex beads (catalog no. 07310; Polysciences, Warrington, PA) were attached to the flagellar stubs as described previously (11). For studies near zero load, the gold spheres were observed by laser dark-field microscopy as described previously (15). For studies at high load, the polystyrene beads were observed by phase-contrast microscopy.

Temperature control

Temperature was controlled to within ± 0.2°C by a Peltier system similar to that described previously (12). The temperature was monitored with a digital thermometer (model no. 91100-20; Cole-Parmer, Vernon Hills, IL) and a small type T thermocouple fixed to the glass slide at a position close to the cells with a drop of silicone oil (510 fluid; Dow Corning, Midland, MI). The thermocouple was calibrated with a mercury thermometer certified by the National Institute of Standards and Technology.

Temperature experiments

A tunnel slide was made from a coverslip coated with poly-L-lysine (catalog no. P4707; Sigma, St. Louis, MO) supported by strips of double sticky tape. A suspension of washed cells was added to the tunnel and incubated for 1 min. Excess cells were then washed away with motility medium. For each experiment, a new tunnel slide was prepared and the speed of one motor was monitored. The temperature in each experiment was varied in the follow sequence: 23.5→ 19.8→ 16.1→ 12.6→ 9.2→ 23.5→ 26.8→ 30.4→ 34.2→ 36.9→ 23.5°C, or sometimes 23.5→ 26.8→ 30.4→ 34.2→ 36.9→ 23.5→ 19.8→ 16.1→ 12.6→ 9.2→ 23.5°C, with 4 min allowed between most settings to ensure that the temperature reached equilibrium, and 9 min allowed for the larger jumps, from 9.2°C or 36.9°C to 23.5°C. The speed measurement at each temperature took 30 s. Sometimes the measurement was repeated to monitor large variations, and the work with any given cell took ≈1 h. Two experiments (on two cells) were performed for each day-culture. The measurement at room temperature (23.5°C) was repeated at least three times (at the beginning, middle, and end of each experiment) to make sure that there was no long-term drift in speed. The speeds from these repetitions usually agreed within $\pm 5\%$. Occasionally, the discrepancies were larger than that, and the experiment was discarded. Experiments in H_2O and D_2O were carried out in the same way.

Isotope effects

A sample of the washed-cell suspension was placed on a glass coverslip coated with poly-L-lysine (as above) and allowed to stand for 5 min. The coverslip was installed as the top window of a flow cell (19) and rinsed with motility medium. The speed of a given motor was measured in H_2O medium (pH 7.0), then in D_2O medium (pD 7.5), and then again in H_2O medium. Media were exchanged (drawn through the flow cell) at a rate of 70 μL/min. For each media exchange, 5 min were allowed to ensure that the system reached equilibrium. In all cases, the flow was continued throughout the experiment. Each speed measurement took ~30 s. These experiments were performed at room temperature (23.5°C).

Data analysis

The anode current from the photomultiplier tube was converted to a voltage that was DC-coupled to an 8-pole low-pass Bessel filter (model 3384; Krohn-Hite, Brockton, MA) with a cutoff frequency of 700 Hz (300 Hz for studies at high loads). The filter output was sampled at 3 kHz (1 kHz for studies at high loads) by a computer data-acquisition system controlled using custom software written in LabVIEW (National Instruments, Austin, TX). Data analysis was done using custom scripts in MATLAB (The MathWorks, Natick, MA). The rotational speed was extracted as the peak of the power spectrum for each 30-s data set. Viscosities of water at different temperatures were taken from the *Handbook of Chemistry and Physics* (20).

RESULTS

Temperature dependence in H_2O near zero load

Nine experiments were carried out in H_2O near zero load (with 60-nm gold spheres on hooks), and the results are shown in Fig. 1 (*solid circles*). Three data points from (10,11) are shown as open circles with error bars. The speed changed nearly exponentially with temperature, as documented further below. The results were also consistent with a previous measurement of the proton permeability of vesicles containing MotA and 60 amino acids from the N-terminus of MotB, where the permeability increased by about a factor of 2.5 when the temperature was increased from 17°C to 27°C (21).

The activation enthalpy can be extracted from an Arrhenius plot of the speeds near zero load. Since there were speed variations among different cells at the same temperature, we extracted the activation enthalpy from each experiment (temperature dependence for a single motor) and then calculated the average over the cell ensemble. Results from a typical experiment are shown in Fig. 2 *A*, and the corresponding Arrhenius plot is shown in Fig. 2 *B*. The activation enthalpies extracted from the nine experiments were 51.3,

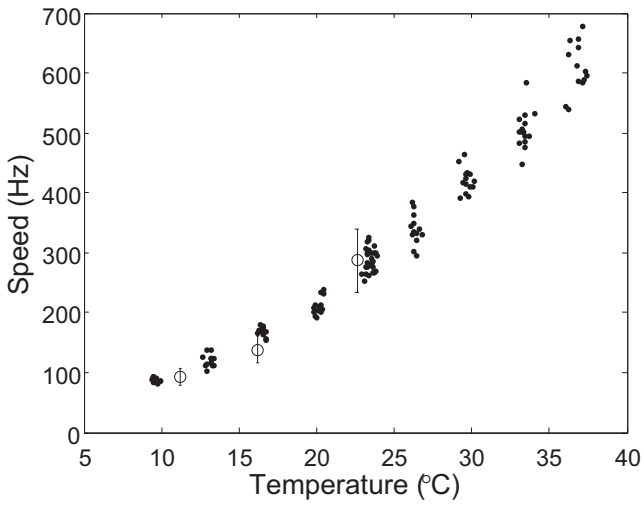

FIGURE 1 Summary plot of speed data near zero load (nine cells; *solid circles*). Three points (*open circles* with error bars) are data from Berg and Turner (10) and Chen and Berg (11).

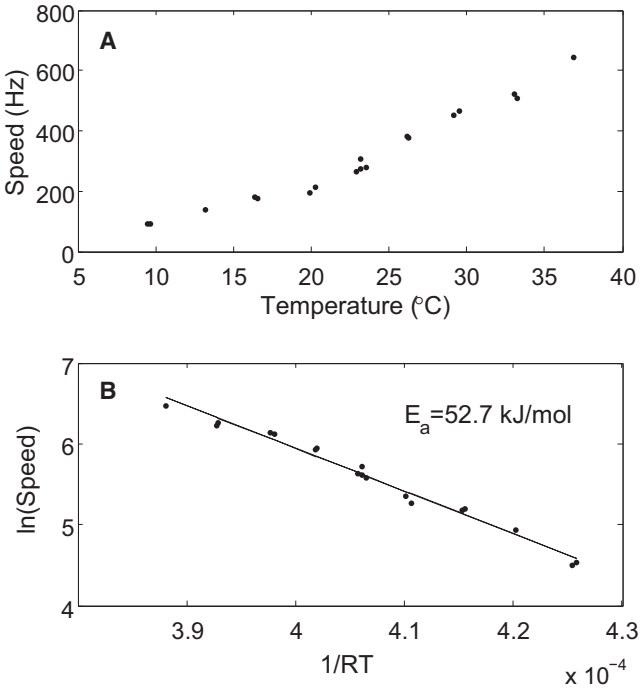

FIGURE 2 Results from a typical experiment on a motor near zero load. (*A*) Speed as a function of temperature. (*B*) The corresponding Arrhenius plot with a linear fit to extract the activation enthalpy (E_a).

53.0, 49.9, 52.7, 50.3, 51.2, 54.0, 55.4, and 46.9 kJ/mol, which led to a mean activation enthalpy ± standard deviation (SD) of 52 ± 3 kJ/mol. Since the rotation speed depends linearly on the proton-motive force (PMF; $\Delta p = \Delta\psi - 2.3(kT/e)\Delta pH$) (13,22,23), possible effects due to variations in PMF have to be considered. *E. coli* maintains its internal pH at ~7.6. For cells grown at pH 7, $\Delta p \approx 170$ and $\Delta\psi \approx 120$ mV at 24°C. For fixed ΔpH, $-2.3(kT/e)$ ΔpH increases by 5.6 mV from 9°C to 37°C, corresponding to a negligible 3% change in PMF. There are no additional substantial changes in PMF, as we demonstrate below using an isogenic strain (containing an additional low-copy-number plasmid expressing the sticky filament) with motors running at high load. Therefore, the observed temperature dependence of motor speed near zero load is a direct effect of temperature on motor kinetics rather than an indirect effect due to variations in PMF.

Temperature dependence at high load

For comparison, and to eliminate possible effects of variations in PMF resulting from changes in temperature, nine experiments were carried out in H_2O at high load (with 1-μm-diameter latex beads on filament stubs; see Fig. 3 (*open circles*) for results). Data were corrected for changes in the viscosity of the medium by multiplying the rotation speeds observed at high load at a given temperature by the ratio of the viscosity of H_2O at that temperature to its viscosity at room temperature (23.5°C). Note that this correction is not required near zero load, where the load remains near zero regardless of modest changes in viscosity. To minimize the effects of speed variance among different cells, the speeds for each experiment were divided by the speed at 23.5°C for that experiment, and averages were taken over the cell ensemble. Results for the zero-load experiments were normalized and averaged in the same way, and are shown in Fig. 3 (*solid circles*). The variations in torque were small at high load (within ±10% in the temperature range of 9–37°C), consistent with previous measurements in which the transmembrane potential was clamped by diffusion of potassium (12) (see below). Since the motor torque at high loads is proportional to the PMF, we were able to assign an upper bound of ±10% to the PMF variations. A 10% increase in torque for the temperature range of 9–37°C corresponds to an activation enthalpy of 2.6 kJ/mol; therefore, we increased the error in activation enthalpy obtained for the zero-load experiments to $\pm(3^2 + 2.6^2)^{1/2} = \pm 4$ kJ/mol.

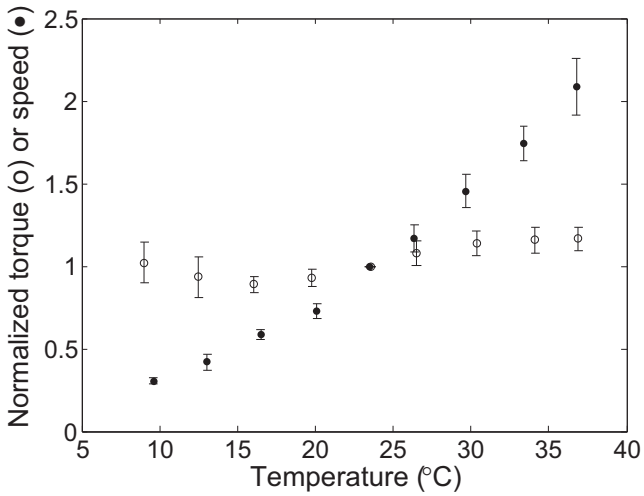

FIGURE 3 Normalized torque or speed as a function of temperature for motors at high load (nine cells, *open circles*) compared with motors near zero load (nine cells; *solid circles*). The normalization procedure is explained in the text.

For the temperature studies at high load (1-μm-diameter latex beads on filament stubs), the filaments had to be quite short before the latex beads were added. When cells were sheared by 30 passages between syringes equipped with 21-gauge needles, the filaments were relatively long, and the torque increased by a factor of ~2 from 9°C to 37°C. When cells were sheared by 70 passages between syringes equipped with 26-gauge needles, as described above, there was almost no increase in torque. We think this difference was due to temperature-dependent changes in the shapes of the longer filaments (possibly polymorphic transformations) that altered the geometry of the load.

Isotope effects at high load

Thirteen motors on different cells were monitored for isotope effects at high load (1-μm-diameter latex beads on filament

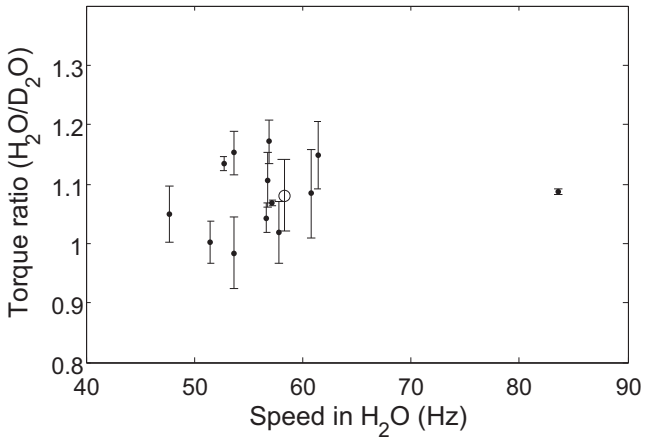

FIGURE 4 Ratio of torque in H_2O medium to that in D_2O medium for 13 motors at high load. Solid circles are the average of torque ratios for each motor using torques in H_2O medium before and after the D_2O measurement, and the error bar was calculated using the difference of torques in H_2O medium before and after the D_2O measurement. The open circle with the error bar is the mean ± SD for all 13 motors (1.08 ± 0.06).

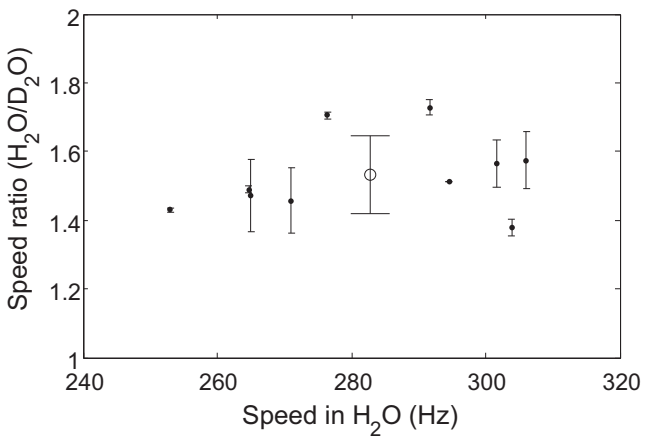

FIGURE 5 Ratio of speed in H_2O medium to that in D_2O medium for 10 motors near zero load. Solid circles are the average of speed ratios for each motor using speeds in H_2O medium before and after the D_2O measurement, and the error bar was calculated using the difference of speeds in H_2O medium before and after the D_2O measurement. The open circle with the error bar is the mean ± SD for all 10 motors (1.53 ± 0.14), including the correction for changes in the deuteron-motive force.

stubs). The motor torque in H_2O medium at pH 7.0 was compared with that in D_2O medium at pD 7.5, following a previously described method (12,14). This use of different pH and pD values compensates for the upward shift in internal pH resulting from changes in the pK_a of weak acids and bases, which are higher in D_2O than in H_2O by ~0.5 (17). The ratios of the torque in H_2O medium to that in D_2O medium are shown in Fig. 4 as a function of motor speeds in H_2O. For each motor, the speeds in H_2O medium before and after the D_2O measurement were averaged ($<v_H>$), and the difference of speeds in H_2O before and after the D_2O measurement was utilized to calculate errors in the torque ratio. Since the viscosity ratio D_2O/H_2O is 1.22 at 23°C, the torque ratio $\tau_H/\tau_D = <v_H>/<v_D>/1.22$. The torques in H_2O were nearly identical to those in D_2O. The mean ± SD of the ratio of the torque in H_2O to that in D_2O for the 13 motors was 1.08 ± 0.06, consistent with previous measurements (14). In an earlier study with tethered cells of *Streptococcus*, in which the transmembrane potential was clamped by diffusion of potassium, the torque ratio was identical to one (0.99 ± 0.02) (12). Therefore, the slight deviation from one in our measurements of the torque ratio suggests that the PMF is slightly larger than the deuteron-motive force, presumably because rates of respiration are larger in H_2O than in D_2O (14). This can serve as a correction of the deuteron-motive force for isotope effects near zero load.

Isotope effects near zero load

Ten motors on different cells were monitored for isotope effects near zero load (60-nm-diameter gold spheres on hooks) in the same manner used for the high-load experiments. Motor speed in H_2O medium at pH 7.0 was compared with that in D_2O medium at pD 7.5. The ratios of the speed in H_2O medium to that in D_2O medium are shown in Fig. 5 as a function of motor speeds in H_2O. For each motor, the speeds in H_2O medium before and after the D_2O measurement were averaged, and the difference of speeds in H_2O before and after the D_2O measurement was utilized to calculate errors in the speed ratio. Data were corrected for the difference between PMF and deuteron-motive force by increasing the speeds in D_2O by a factor of 1.08 ± 0.06. The mean ± SD of the ratio of the speed in H_2O to that in D_2O for the 10 motors was 1.53 ± 0.14 (1.65 ± 0.15 without correction for the deuteron-motive force).

Temperature dependence near zero load in D_2O

Ten experiments were carried out in D_2O near zero load (60-nm-diameter gold spheres on hooks). The speeds for each experiment were divided by the speed at 23.5°C for that experiment, and averages were taken over the cell ensemble. Results are shown in Fig. 6 (*solid circles*). Results for temperature dependence in H_2O medium near zero load were normalized in a similar manner and included for comparison (*open circles*). The changes in speed relative to those at 23.5°C were nearly identical in D_2O and H_2O. The activation enthalpies extracted from the 10 experiments in D_2O were 55.1, 50.6, 46.4, 45.6, 59.1, 47.7, 51.0, 50.9, 48.3, and 47.7 kJ/mol, which led to a mean activation enthalpy ± SD of 50 ± 4 kJ/mol for the cell ensemble, close to the activation enthalpy of 52 ± 4 kJ/mol measured in H_2O medium.

DISCUSSION

We found that near zero load, motor speed increases nearly exponentially with temperature, exhibiting the same

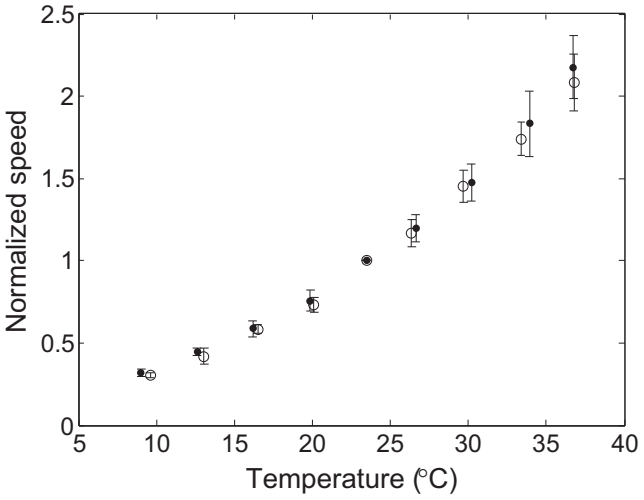

FIGURE 6 Normalized speed as a function of temperature for motors near zero load in D_2O medium (10 cells; *solid circles*) compared with motors near zero load in H_2O medium (nine cells; *open circles*). The normalization procedure is explained in the text.

activation enthalpy in H_2O (52 ± 4 kJ/mol) as in D_2O (50 ± 4 kJ/mol). The H_2O/ D_2O speed ratio at 23.5°C was 1.53 ± 0.14. At high load, the motor torque was independent of temperature and solvent-isotope effects were negligible, in agreement with previous work (12,14).

The residue Asp-32 of MotB, found near the cytoplasmic end of the proton channel, is known to be critical for proton transfer (8). Protonation and subsequent deprotonation of Asp-32 are thought to drive conformational changes within the stator that exert forces on the periphery of the rotor (9). The pK_a values of most carboxylic and ammonium acids increase in D_2O by ~0.5 (17) because deuterons generally are held more tightly than protons. If deprotonation of Asp-32 were the rate-limiting step near zero load, the speed in D_2O would decrease by a factor of $(D_H/D_D) \times 10^{0.5} = 4.4$ relative to the speed in H_2O, where $D_H/D_D \approx 1.4$ is the ratio of H^+ and D^+ diffusion coefficients in aqueous solutions (24). The factor measured in this work, 1.53 ± 0.14, is substantially smaller, suggesting that deprotonation of Asp-32 is not the rate-limiting step. However, this does not rule out the possibility that deprotonation of Asp-32, while rate-limiting, involves proton transfer to a nearby group rather than escape to the cytoplasm (see below).

The large dependence of speed on temperature, the large solvent-isotope effect, and the simple ohmic current-PMF relation measured previously (22,23) are characteristic of open voltage-gated proton channels (25,26). Proton pathways in these channels are usually formed by water molecules and titratable amino acid side chains, and protons translocate by a hydrogen-bonded chain mechanism by hopping from one water or titratable group to the next (27). Proton translocation in the flagellar motor may involve a similar mechanism.

However, the exponential dependence of speed on temperature shown in Figs. 1 and 6, and as an Arrhenius plot in Fig. 2, is consistent with a single rate-limiting step (a single barrier-crossing event). According to Eyring's transition-state theory for an elementary chemical reaction, the forward rate $v = (kT/h)\exp(-\Delta G_a/RT)$, where k and h are the Boltzmann and Planck constants, respectively. If we assume from energy considerations and the duplication of proton channels that two protons pass through each force-generating unit every step (2), that there are 26 steps per revolution (28), and that the zero-load speed is ~300 Hz (15), then the proton flux (or reaction rate) v is $\sim 2\times 26\times 300\ s^{-1}$. From Eyring's equation, this leads to an activation energy of ~50 kJ/mol, which is the same as the activation enthalpy obtained from the temperature dependence of zero-load speed. This indicates, in Eyring's theory, that the entropy of activation is small. An alternative model is that of Kramers, in which the frequency factor kT/h is replaced by one estimated from global diffusion of the protein into the activated state (29). In either case, the exponential dependence implies that an elementary step in the proton pathway might be rate-limiting. A recent study by Kim et al. (7) provided a possible candidate for the rate-limiting elementary step: formation of a hydrogen bond from the protonated MotB Asp-32 to carbonyl-169 of MotA to cause bending of the MotA helix.

Our measurement of the deuterium solvent-isotope effect of 1.53 further supports the idea that proton transfer from MotB Asp-32 to carbonyl-169 of MotA might be the rate-limiting step. If this transfer is like proton transfer in water, we might expect a deuterium solvent-isotope effect similar to the ratio of H^+ and D^+ diffusion coefficients in aqueous media, i.e., ~1.4 (24), which is close to our measurement of 1.53. A complete understanding of the proton pathway and rate-limiting steps await atomic-level resolution of MotA and MotB structures.

We thank Y. Tu and J. Xing for helpful discussions.

This work was supported by National Institutes of Heath grant AI016478.

REFERENCES

1. Berg, H. C. 2003. The rotary motor of bacterial flagella. *Annu. Rev. Biochem.* 72:19–54.
2. Blair, D. F. 2003. Flagellar movement driven by proton translocation. *FEBS Lett.* 545:86–95.
3. Blair, D. F., and H. C. Berg. 1991. Mutations in the MotA protein of *Escherichia coli* reveal domains critical for proton conduction. *J. Mol. Biol.* 221:1433–1442.
4. Sharp, L. L., J. Zhou, and D. F. Blair. 1995. Features of MotA proton channel structure revealed by tryptophan-scanning mutagenesis. *Proc. Natl. Acad. Sci. USA.* 92:7946–7950.
5. Sharp, L. L., J. Zhou, and D. F. Blair. 1995. Tryptophan-scanning mutagenesis of MotB, an integral membrane protein essential for flagellar rotation in *Escherichia coli*. *Biochemistry.* 34:9166–9171.
6. Braun, T. F., L. Q. Al-Mawsawi, …, D. F. Blair. 2004. Arrangement of core membrane segments in the MotA/MotB proton-channel complex of *Escherichia coli*. *Biochemistry.* 43:35–45.

7. Kim, E. A., M. Price-Carter, …, D. F. Blair. 2008. Membrane segment organization in the stator complex of the flagellar motor: implications for proton flow and proton-induced conformational change. *Biochemistry*. 47:11332–11339.
8. Zhou, J., L. L. Sharp, …, D. F. Blair. 1998. Function of protonatable residues in the flagellar motor of *Escherichia coli*: a critical role for Asp 32 of MotB. *J. Bacteriol.* 180:2729–2735.
9. Kojima, S., and D. F. Blair. 2001. Conformational change in the stator of the bacterial flagellar motor. *Biochemistry*. 40:13041–13050.
10. Berg, H. C., and L. Turner. 1993. Torque generated by the flagellar motor of *Escherichia coli*. *Biophys. J.* 65:2201–2216.
11. Chen, X., and H. C. Berg. 2000. Torque-speed relationship of the flagellar rotary motor of *Escherichia coli*. *Biophys. J.* 78:1036–1041.
12. Khan, S., and H. C. Berg. 1983. Isotope and thermal effects in chemiosmotic coupling to the flagellar motor of *Streptococcus*. *Cell.* 32:913–919.
13. Meister, M., G. Lowe, and H. C. Berg. 1987. The proton flux through the bacterial flagellar motor. *Cell.* 49:643–650.
14. Chen, X., and H. C. Berg. 2000. Solvent-isotope and pH effects on flagellar rotation in *Escherichia coli*. *Biophys. J.* 78:2280–2284.
15. Yuan, J., and H. C. Berg. 2008. Resurrection of the flagellar rotary motor near zero load. *Proc. Natl. Acad. Sci. USA*. 105:1182–1185.
16. Yuan, J., K. A. Fahrner, and H. C. Berg. 2009. Switching of the bacterial flagellar motor near zero load. *J. Mol. Biol.* 390:394–400.
17. Schowen, K. B., and R. L. Schowen. 1982. Solvent isotope effects of enzyme systems. *Methods Enzymol.* 87:551–606.
18. Parkinson, J. S. 1978. Complementation analysis and deletion mapping of *Escherichia coli* mutants defective in chemotaxis. *J. Bacteriol.* 135:45–53.
19. Berg, H. C., and S. M. Block. 1984. A miniature flow cell designed for rapid exchange of media under high-power microscope objectives. *J. Gen. Microbiol.* 130:2915–2920.
20. Weast, R. C., M. J. Astle, and W. H. Beyer, editors. 2008–2009. CRC Handbook of Chemistry and Physics. CRC Press, Boca Raton, FL.
21. Blair, D. F., and H. C. Berg. 1990. The MotA protein of *E. coli* is a proton-conducting component of the flagellar motor. *Cell.* 60: 439–449.
22. Gabel, C. V., and H. C. Berg. 2003. The speed of the flagellar rotary motor of *Escherichia coli* varies linearly with protonmotive force. *Proc. Natl. Acad. Sci. USA*. 100:8748–8751.
23. Lo, C. J., M. C. Leake, …, R. M. Berry. 2007. Nonequivalence of membrane voltage and ion-gradient as driving forces for the bacterial flagellar motor at low load. *Biophys. J.* 93:294–302.
24. Kohen, A. and H. Limbach, editors. 2006. Isotope Effects in Chemistry and Biology. CRC Press, Boca Raton, FL.
25. DeCoursey, T. E., and V. V. Cherny. 1998. Temperature dependence of voltage-gated H^+ currents in human neutrophils, rat alveolar epithelial cells, and mammalian phagocytes. *J. Gen. Physiol.* 112:503–522.
26. Decoursey, T. E. 2003. Voltage-gated proton channels and other proton transfer pathways. *Physiol. Rev.* 83:475–579.
27. Nagle, J. F., M. Mille, and H. J. Morowitz. 1980. Theory of hydrogen bonded chains in bioenergetics. *J. Chem. Phys.* 72:3959–3971.
28. Sowa, Y., A. D. Rowe, …, R. M. Berry. 2005. Direct observation of steps in rotation of the bacterial flagellar motor. *Nature*. 437:916–919.
29. Howard, J. 2001. Mechanics of Motor Proteins and the Cytoskeleton. Sinauer Associates, Sunderland, MA. 83–88.